BIOLOGY OF REPRODUCTION (2013) **88**(2):52, 1–13
Published online before print 9 January 2013.
DOI 10.1095/biolreprod.112.104802

Targeted Genome-Wide Methylation and Gene Expression Analyses Reveal Signaling Pathways Involved in Ovarian Dysfunction after Developmental EDC Exposure in Rats[1]

Aparna Mahakali Zama and Mehmet Uzumcu[2]

Department of Animal Sciences, School of Environmental and Biological Sciences, Rutgers, The State University of New Jersey, New Brunswick, New Jersey

ABSTRACT

Transient exposure to methoxychlor (MXC), an environmental endocrine-disrupting chemical, during fetal and neonatal stages causes ovarian dysfunction in pubertal, adult, and aging animals. Adult animals have reduced number of ovulations and abnormal follicular composition associated with altered gene expression and DNA methylation patterns. To test the hypothesis that the ovarian epigenomic changes induced by MXC are detectable following the exposure period, leading to altered gene expression by adulthood, we conducted a targeted genome-wide methylation study using Nimblegen 3x720K CpG Island Plus RefSeq Promoter Arrays. Control (vehicle), low-dose MXC (20 μg/kg/day), or high-dose MXC (100 mg/kg/day) treatments were administered between Embryonic Day 19 and Postnatal Day (PND) 7. Ovaries were collected at PND 7 immediately after exposure or at adulthood, PND 60. Array hybridizations were conducted with genomic DNA after methylated DNA immunoprecipitation and the array data were analyzed. DNA methylation events were functionally annotated, and candidate loci common to all the treatments or unique to some treatments were identified. Specific loci encoding signaling molecules such as the regulatory subunit p85 of phosphoinositide-3-kinase, insulin-like growth factor-1 receptor, Harvey rat sarcoma viral oncogene, insulin receptor, and forkhead box protein O3 were identified to be hypermethylated in MXC-treated ovaries at PND 7 and/or PND 60. Examination of gene expression changes with TaqMan low-density arrays revealed that nearly 25% of the genes that were assayed were downregulated. These data demonstrate that key molecules in specific signaling pathways such as PTEN signaling, IGF-1 signaling, or rapid estrogen signaling are epigenetically altered in MXC-exposed ovaries, which is associated with ovarian dysfunction and female infertility.

development, endocrine-disrupting chemicals, epigenetics, folliculogenesis, functional annotation, gene expression, methylation, ovary

INTRODUCTION

The developmental origins of health and disease concept suggests the existence of a period of high vulnerability to various adverse environmental conditions during early development that when perturbed could lead to diseases in adulthood (developmental programming, see reviews [1–3]). Our previous work [4–6] has demonstrated that transient exposure to the pesticide methoxychlor (MXC), an environmental endocrine-disrupting chemical (EDC), during fetal and neonatal stages of development affected multiple female reproductive parameters in pubertal, adult, and aging animals. More specifically, exposure of female rats to MXC during a critical period of ovarian development, from Embryonic Day (E) 19 through Postnatal Day (PND) 7, resulted in 1) accelerated puberty and first estrous cycle, 2) subsequent irregular cyclicity, 3) reduced litter size, 4) reduced superovulatory response to gonadotropins, 5) increased circulating levels of LH and reduced levels of estradiol and progesterone, and 6) premature reproductive aging [4]. This phenotype was very similar to the symptoms seen in women who had been exposed to agricultural pesticides: prolonged/irregular estrous cycles, difficulty in achieving pregnancy, failed in vitro fertilization attempts, and loss of pregnancies [7, 8].

We found that the hallmark defects associated with MXC exposure related to ovarian dysfunction were reduced number of ovulations and abnormal follicular composition. The basis of these defects was elucidated by immunohistochemical analysis of gene expression patterns at PND 60 [4], and collectively, these studies suggested that signaling pathways involved in follicular progression, maturation, and ovulation were probably affected. Furthermore, a recent study has shown that neuroendocrine gene expression and DNA methylation of estrogen receptor-1 (*Esr1*) gene were altered due to MXC exposure [6].

The overall female reproductive lifespan is dependent on the orderly progression of the early stages of folliculogenesis. Primordial follicles are assembled following oocyte nest breakdown. Once formed, some of the follicles are activated while most are initially quiescent, to be activated throughout reproductive life by a process known as the initial recruitment or the primordial-to-primary follicle transition. Recruitment into the growing cohort of primary follicles relies on complex bidirectional communication between the oocyte and its surrounding somatic cells and involves stimulatory inputs from local paracrine factors as well as steroid hormones [9–11]. Recent studies have suggested that a reduction in the levels of ovarian steroids following birth is necessary for oocyte nest breakdown and follicular assembly and that these processes are disrupted by exposure to estrogenic compounds such as diethylstilbestrol, genistein, or bisphenol-A (BPA) during the early neonatal period, resulting in multiovular

[1]Supported by National Institutes of Health grants ES013854, ES017059, and P30ES005022. Presented in part at the 44th Annual Meeting of the Society for the Study of Reproduction, July 31–August 4, 2011, Portland, Oregon.
[2]Correspondence: Mehmet Uzumcu, Department of Animal Sciences, School of Environmental and Biological Sciences, Rutgers, The State University of New Jersey, 84 Lipman Drive, New Brunswick, NJ 08901-8525. E-mail: uzumcu@aesop.rutgers.edu

Received: 13 September 2012.
First decision: 3 October 2012.
Accepted: 4 January 2013.

eISSN: 1529-7268 http://www.biolreprod.org
ISSN: 0006-3363

follicles (MOFs) [3, 9, 10, 12–14]. Because MXC can exert estrogenic or anti-estrogenic activity depending on the type of metabolites it produces as demonstrated previously [15, 16], it is imperative to investigate whether MXC can alter early follicular assembly and/or subsequent progression of folliculogenesis.

Many recent studies have suggested that environmental exposure and subsequent disease outcomes reflect the interplay between an individual's epigenetic composition and the environment [5, 6, 17, 18]. Epigenetic mechanisms can be affected by EDCs during major epigenetic reprogramming events (e.g., erasure and reestablishment of DNA methylation patterns of imprinted genes in germ cells) [3]. In rodents, the germ cell genome that is normally methylated prior to migrating to the genital ridge is unmethylated after migration, including at imprinted loci [19]. Subsequently, remethylation, which is mediated through an interaction between somatic and germ cells, occurs in a sex-specific manner at different developmental stages [20]. In mice, while male germ cell remethylation starts at E14 and is mostly complete by E16–E17 [21, 22], female germ cell remethylation is initiated during the postnatal period PND 1–5 (the same period as follicular assembly and initial recruitment) and continues throughout oocyte growth until the preantral follicle stage [23]. Methoxychlor exposure leads to both hypermethylation and hypomethylation in imprinted loci in mouse sperm [24]. It is possible that MXC can also alter DNA methylation patterns in somatic cells during ovarian development. Therefore, we hypothesized that because the MXC exposure window in our studies was during early folliculogenesis, any disruption in the ovarian epigenome at this stage could lead to altered gene expression by adulthood.

In a previous study, DNA from adult female rats that were exposed to MXC in the fetal and neonatal stages was assayed. The arbitrarily primed PCR after HpaII digestion (AP-PCR) technique was conducted, and 10 hypermethylated loci involved in ovarian function were identified [5]. Assays such as AP-PCR depend on the availability of restriction enzyme sites, thereby leaving a possibility that all the methylation events may not be captured. Furthermore, because DNA methylation is dynamic and reversible [25], the objective of the current study was to conduct a genome-wide analysis to identify multiple signaling pathways that could potentially be regulated by DNA methylation. In addition, in our previous study, we found lowered expression of ESR2 and hypermethylation of the *Esr2* promoter, an observation that was implicated in the overall phenotype of the MXC-exposed ovaries [5]. However, when we examined the gene expression and methylation pattern of *Esr2* at PND 7, we found that there were no significant changes in either (Zama and Uzumcu, unpublished results). These data led us to further hypothesize that the genes that have altered methylation patterns immediately after exposure may not be the same as the genes affected later in adulthood.

To test our hypotheses, we conducted targeted genome-wide methylation analyses in both promoter and RefSeq regions at two different ages, 1) immediately after exposure at PND 7 and 2) after animals reach adulthood, PND 60, when the exposed animals exhibit characteristic defects. Our current approach enabled us to examine not only individual gene methylation patterns but also potential gene networks that were exhibiting altered methylation patterns in response to EDC exposure, both at proximate and more latent times relative to the exposure.

MATERIALS AND METHODS

Animals and Treatments

Eight- to twelve-week-old Fischer CDF female rats (Charles River) were maintained on a 14L:10D cycle and fed, ad libitum, a reduced isoflavone diet (Purina) in order to minimize possible effects of phytoestrogens. The estrous cycles of the rats were followed daily, and individual females were mated with untreated males starting on proestrus. A sperm-positive vaginal smear was designated E0. The timed-pregnant females received one of two different treatment dosages of MXC (Sigma): 20 μg/kg/day (low-dose MXC) and 100 mg/kg/day (high-dose MXC) in 1 ml/kg vehicle. Control animals received only vehicle (dimethylsulfoxide [DMSO]: sesame oil [1:2], control). The 20 μg/kg/day MXC dose is considered to be an environmentally relevant dose of MXC while the 100 mg/kg/day MXC dose represents the midrange of doses of MXC that have been used in many past studies in this laboratory and others [26–28].

Daily treatments were administered intraperitoneally to the pregnant dams between E19 and E22 and subcutaneously (in the folds of the neck) to the neonates within 8 h of birth (considered PND 0) and continued until PND 7. For the early folliculogenesis studies, pups were euthanized 8 h after treatment on PND 7 via decapitation. For the adult studies, females were followed for estrous cyclicity and euthanized between PND 50 and 60 (named PND 60) on proestrus day after their third cycle. All the animal care and treatment protocols were carried out in accordance with institutional guidelines and were approved by Rutgers Animal Care and Facilities Committee.

Collection of Ovaries

The PND 7 ovaries were microscopically dissected, fixed in Bouin fixative for 2 h, washed in 70% ethanol, and processed for paraffin embedding for further histological analysis. Ovaries from PND 7 and 60 females were fine dissected, snap frozen, and processed for nucleic acid extractions and used for methylation and gene expression analyses (see below). Ovaries from three animals (from three different litters) of each treatment at PND 7 and PND 60 (total 18 samples) were utilized for the methylation analyses as well as gene expression analyses, while ovaries from five to seven animals (from at least three separate litters) were used for each of the three treatment groups in follicular composition analysis, immunohistochemistry (IHC), and quantification of staining intensities.

Classification of Follicles

Paraffin blocks were sectioned at 5 μm, and the sections were stained with hematoxylin and eosin (H and E) (Fisher Scientific). All the follicles and oocyte nests were counted in the entire section. The follicles were classified into different follicular stages in two serial sections from the largest cross-sections through the center of the ovary and averaged as previously described, which was shown to represent the entire ovary [29, 30]. Briefly, oocyte nests are unassembled oocytes in aggregates of two to four oocytes, and primordial follicles are follicles containing an oocyte surrounded by squamous granulosa cells with no more than one cuboidal granulosa cell. Early primary follicles have a larger oocyte that is surrounded by an incomplete layer of cuboidal granulosa cells. The primary stage contains the growing oocyte surrounded by a complete layer of cuboidal granulosa cells and some newly recruited theca cells. Finally, transitional/secondary follicles contain the oocyte surrounded by two or more layers of granulosa cells and a growing theca layer [29]. One-way ANOVA with the Dunnett posttest was used to assess differences between control and treated ovaries in the total number of follicles present and the percentage of follicles in each developmental stage. A $P < 0.05$ was considered to be significant.

Immunohistochemistry

Immunohistochemical analysis was conducted as previously described [4, 5]. Briefly, anti-MIS antibody (200 μg/ml goat polyclonal, SC-6886, Santa Cruz Biotechnology) was utilized at a 1:100 dilution on Bouin-fixed sections. Biotinylated anti-goat secondary IgG antibody (200 μg/0.5 ml, Santa Cruz Biotechnology) and streptavidin-fluorescein isothiocyanate (SA-5001, Vector Laboratories) were used for secondary detection. All the sections were also stained with ethidium homodimer (E3599; Life Technologies) as a nuclear counterstain (not shown) and mounted in Prolong Gold anti-fade reagent (P36934; Life Technologies). Sections of negative controls were treated identically, except that the primary antibody was replaced with PBS. Sections were observed under a Nikon Eclipse E800 microscope with epifluorescence attachments, and images were acquired with a Nikon DXM1200F camera with ACT1 software at the same exposure. The immunostaining intensities were

quantified using Image J software (National Institutes of Health [NIH]). One-way ANOVA with the Dunnett posttest was used to assess the staining intensity for IHC. A $P < 0.05$ was considered to be significant.

Methylated DNA Immunoprecipitation

High-quality genomic DNA was extracted from ovaries using the phenol:chloroform:isoamyl alcohol method. Six micrograms of genomic DNA was restriction-digested with the frequent cutter, MseI (T↓TAA) (New England Biolabs), an enzyme that does not typically cut in GC-rich regions, and 200-1000 bp fragments were obtained. They were purified (Qiagen) and quantified using a NanoDrop spectrophotometer (Thermo Fisher Scientific). Verification of fragment size was conducted by gel electrophoresis before heat denaturation and snap cooling to facilitate single strand formation. An aliquot was reserved after quantification for use as control (input DNA). The remainder was immunoprecipitated with 1 μg of anti-5-methyl-cytidine antibody (Abcam). The DNA-antibody complexes were captured using Protein-A agarose beads (Invitrogen), washed to remove nonspecific binding, and the DNA separated/eluted by proteinase K digestion. Phenol:chloroform extraction and ethanol precipitation were then performed, and methylated DNA immunoprecipitation (MeDIP) DNA was quantitated. All the MeDIP DNA amounts were in the 5–10 ng/μl range. Whole-genome amplification (WGA; Sigma) was conducted with a starting amount of 10 ng/μl for both input and MeDIP DNA as per manufacturer's instructions. The WGA-amplified DNA was purified (Qiagen), and 4 μg was utilized for array hybridization.

Array Design, Hybridization, and Analysis

The input and MeDIP fractions were differentially labeled (Cy3 and Cy5, respectively) and hybridized to the Nimblegen 3x720K CpG Island Plus RefSeq Promoter Arrays. These cover the CpG islands as well as the promoters of well-characterized RefSeq genes; 3.88 kb upstream and 0.97 kb downstream of promoters were covered as well as 15 600 transcripts, 15 287 promoters, and 15 790 CpG islands. Repetitive regions were excluded and non-CpG intragenic and intergenic regions were not covered. The probe lengths were between 50–75 mer. Array data were analyzed using Nimblescan software (Nimblegen Inc.) as part of our service agreement, details of which are available on www.Nimblegen.com. Briefly, the four important parts of the analysis were as follows. First, the signal intensity was extracted from the scanned images of each array. Second, the scaled $\log_2$ ratio data for each feature on the array was calculated as the ratio of the MeDIP and input samples cohybridized to the array scaled to center the ratio data around zero. Centering was performed by subtracting the biweight mean for the $\log_2$ ratio values for all the features on the array from each $\log_2$ ratio value. Third, from the scaled $\log_2$ ratio data, a fixed-length window of 750 bp was placed around each consecutive probe and the one-sided Kolmogorov-Smirnov (KS) test was applied to determine whether the probes were drawn from a significantly more positive distribution of intensity log ratios than those in the rest of the array. The resulting score for each probe was the $-\log_{10}$ transformed P value from the windowed KS test around that probe. Finally, the peak data files were generated from the P-value data by searching for two probes at a time above our specified P-value minimum cutoff of ≥ 2, and the peaks merged within a 500 bp distance of each other. In this manner, an average of ~3000 methylation peaks were identified in each individual sample. Functional annotation was performed using Ingenuity Pathway Analysis (IPA) (Ingenuity Systems, www.ingenuity.com).

Functional Annotation Using IPA

Candidates were functionally annotated after core analysis was conducted on each sample from each treatment group wherein loci had ≥2.00 assigned peak score in Nimblescan. Comparison analyses between animals of the same treatment group were performed for the presence of candidate hits in all three replicate samples of each treatment, and the resultant common group was used as the working representative list for that group. In the next step, unique methylation events to specific treatment groups and those common to all the treatment groups were identified. Canonical pathways analysis identified the pathways from the IPA library of canonical pathways that were most significant to the data set. Molecules from the data set that met the >2 peak score cutoff that were associated with a canonical pathway in Ingenuity Knowledge Base were considered for the analysis. The significance of the association between the data set and the canonical pathway was measured in two ways. First, a ratio of the number of molecules from our data sets that map to the pathway was divided by the total number of molecules that map to the canonical pathway. Second, the Fisher exact test was used to calculate a P value indicating the probability that the association between the genes in the dataset and the canonical pathway is explained by chance alone. A $P < 0.05$ was considered significant and set as the threshold.

RNA Extractions and Whole Transcriptome Amplification

Because of the limited quantities of RNA for gene expression analysis obtained from PND 7 ovaries, total RNA was extracted (Qiagen RNEasy extraction kit) and 50 ng was converted to cDNA using the Nugen Applause WT-Amp ST system (Nugen Inc.) as per the manufacturer's instructions. Because cross comparisons between PND 7 and PND 60 ovaries were conducted, PND 60 mRNA was also amplified.

TaqMan Low-Density Array Analysis

The complete list of all the genes was assayed using TaqMan low-density array (TLDA) (Supplemental Table S1; all the supplemental data are available online at www.biolreprod.org). Candidates were selected if they were unique to either of the doses, but preferentially the high dose, at either PND 7 or 60. In addition, genes that were considered to be relevant to the specific pathways of these hypermethylated loci were also examined. For example, *Esr1* was hypermethylated at PND 7 (Table 1). We, therefore, not only examined the gene expression changes of *Esr1* but also included *Arnt* (Supplemental Table S1) that was not a hypermethylated locus, yet is a well-known regulator of the *Esr1* signaling pathway in EDC-exposed ovaries [31, 32]. Complementary DNA was loaded on custom-made, 384-well, 96-gene TLDA microfluidic cards and run on an ABI 7900 Fast real-time PCR machine. Three different endogenous control genes, *18S,* β-actin, and β2-microglobulin were included. Samples were run in duplicates. Relative gene expression was analyzed using the Comparative Ct method. The control group (n = 3) within each age group was used as the calibrator group (Data Assist Software; Applied Bio Systems), and the false discovery rate was calculated (Benjamini-Hochberg method, $P < 0.05$). A secondary t-test (two-tailed, nonparametric) was performed and P values reported.

RESULTS

Dose-Dependent Immediate Effect of MXC on Neonatal Folliculogenesis

Our previous studies examined the effects of fetal and neonatal exposure to MXC on adult ovaries [4, 5]. However, immediate effects on PND 7 ovaries were not known. To assess these, we examined H and E stained histology of ovaries from PND 7 animals treated between E19 and PND 7 (Fig. 1). The control ovaries (Fig. 1A) contained all of the developmental stages from primordial follicles up to and including secondary follicles with very few oocyte nests while the low-dose MXC-treated ovaries (Fig. 1B) appeared to have an increased number of oocyte nests and primordial follicles as compared to the control. The high-dose MXC-treated ovaries (Fig. 1C) had a larger number of transitional and secondary stage follicles compared to the control ovaries.

Altered Follicular Composition

To confirm these observations, we conducted an analysis of follicular stage distribution. All the follicle counts were expressed as a percentage of the total number of follicles. The fetal and neonatal treatment with low-dose MXC resulted in a 2.5-fold increase in the percentage of oocyte nests (Fig. 1D; from 2.6% to 6.7%, $P < 0.01$) and a significant increase in the percentage of primordial follicles (Fig. 1E; from 47.3% to 56.0%, $P < 0.01$) at PND 7. There was a concomitant decrease in the percentage of early primary follicles (Fig. 1F; from 25.7% to 15.4%, $P < 0.01$). High-dose MXC treatment generated a significant decrease in the percentage of primordial follicles (Fig. 1E; from 47.3% to 39.8%, $P < 0.01$), accompanied by a nearly 2-fold elevation in the percentage of transitional/secondary follicles per section of PND 7 ovaries (Fig. 1H; from 16.1% to 29.5%, $P < 0.01$). As seen in Figure 1I, the overall total number of follicles per sectional area was not altered by any of the treatments.

Upregulation of AMH Expression

AMH expression was used as a marker to evaluate the progression of folliculogenesis, Transitional and secondary

TABLE 1. The genes that were hypermethylated in PND 7 ovaries by fetal and neonatal exposures to low dose (20 μg/kg) and high dose (100 mg/kg) of MXC.

Symbol	Entrez gene name	Location	Type(s)	Entrez gene ID for rat
High dose MXC				
Accn3	Amiloride-sensitive cation channel 3	Plasma membrane	Ion channel	286920
Clec11a	C-type lectin domain family 11, member A	Extracellular space	Growth factor	29313
Cyp26b1	Cytochrome P450, family 26, subfamily B, polypeptide 1	Cytoplasm	Enzyme	312495
Dctn2	Dynactin 2 (p50)	Cytoplasm	Other	299850
Eif4e	Eukaryotic translation initiation factor 4E	Cytoplasm	Translation regulator	117045
Esr1	Estrogen receptor 1	Nucleus	Ligand-dependent nuclear receptor	24890
Exoc4	Exocyst complex component 4	Cytoplasm	Transporter	116654
Filip1	Filamin A interacting protein 1	Cytoplasm	Other	246776
Hcn4	Hyperpolarization activated cyclic nucleotide-gated potassium channel 4	Plasma membrane	Ion channel	59266
Hsp90aa1	Heat shock protein 90kDa alpha (cytosolic), class A member 1	Cytoplasm	Enzyme	299331
Igf1	Insulin-like growth factor 1 (somatomedin C)	Extracellular space	Growth factor	24482
Il24	Interleukin 24	Extracellular space	Cytokine	170819
Kcna2	Potassium voltage-gated channel, shaker-related subfamily, member 2	Plasma membrane	Ion channel	25468
Kif5a	Kinesin family member 5A	Cytoplasm	Transporter	314906
Klc1	Kinesin light chain 1	Cytoplasm	Other	171041
Lcn2	Lipocalin 2	Extracellular space	Transporter	170496
Lpar1	Lysophosphatidic acid receptor 1	Plasma membrane	G-protein coupled receptor	116744
Magi2	Membrane associated guanylate kinase, WW and PDZ domain containing 2	Plasma membrane	Kinase	113970
Nr4a3	Nuclear receptor subfamily 4, group A, member 3	Nucleus	Ligand-dependent nuclear receptor	58853
Numbl	Numb homolog (*Drosophila*)-like	Cytoplasm	Other	292732
Shank1	SH3 and multiple ankyrin repeat domains 1	Cytoplasm	Other	78957
Siah2	Seven in absentia homolog 2 (*Drosophila*)	Nucleus	Transcription regulator	140593
Stub1	STIP1 homology and U-box containing protein 1, E3 ubiquitin protein ligase	Cytoplasm	Enzyme	287155
Tgfbr1	Transforming growth factor, beta receptor 1	Plasma Membrane	Kinase	29591
Trpc4	Transient receptor potential cation channel, subfamily C, member 4	Plasma membrane	Ion channel	84494
Low dose MXC				
Adra1b	Adrenergic, alpha-1B-, receptor	Plasma membrane	G-protein coupled receptor	24173
Atp5b	ATP synthase, H+ transporting, mitochondrial F1 complex, beta polypeptide	Cytoplasm	Transporter	171374
Cacnb2	Calcium channel, voltage-dependent, beta 2 subunit	Plasma membrane	Ion channel	116600
Camkk2	Calcium/calmodulin-dependent protein kinase kinase 2, beta	Cytoplasm	Kinase	83506
Cav1	Caveolin 1, caveolae protein, 22kDa	Plasma membrane	Other	25404
Cdc42ep5	CDC42 effector protein (Rho GTPase binding) 5	Cytoplasm	Other	361505
Chga	Chromogranin A (parathyroid secretory protein 1)	Extracellular space	Other	24258
Cntnap1	Contactin associated protein 1	Plasma membrane	Other	84008
Dgkz	Diacylglycerol kinase, zeta	Cytoplasm	Kinase	81821
Dync1li1	Dynein, cytoplasmic 1, light intermediate chain 1	Cytoplasm	Other	252902
Gipc1	GIPC PDZ domain containing family, member 1	Cytoplasm	Other	83823
Gphn	Gephyrin	Plasma membrane	Enzyme	64845
Hras	v-Ha-ras Harvey rat sarcoma viral oncogene homolog	Plasma membrane	Enzyme	293621
Hspe1	Heat shock 10kDa protein 1 (chaperonin 10)	Cytoplasm	Enzyme	25462
Iqub	IQ motif and ubiquitin domain containing	Cytoplasm	Other	296936
Irs1	Insulin receptor substrate 1	Cytoplasm	Other	25467
Itgam	Integrin, alpha M (complement component 3 receptor 3 subunit)	Plasma membrane	Other	25021
Jup	Junction plakoglobin	Plasma membrane	Other	81679
Kcnma1	Potassium large conductance calcium-activated channel, subfamily M, alpha member 1	Plasma membrane	Ion channel	83731
Klhl17	Kelch-like 17 (*Drosophila*)	Cytoplasm	Other	246757
Lgals3	Lectin, galactoside-binding, soluble, 3	Extracellular space	Other	83781
Mobkl3	MOB1, Mps One Binder kinase activator-like 3 (yeast)	Cytoplasm	Other	171050
Nck1	NCK adaptor protein 1	Cytoplasm	Kinase	300955
Ntrk2	Neurotrophic tyrosine kinase, receptor, type 2	Plasma membrane	Kinase	25054
Onecut1	One cut homeobox 1	Nucleus	Transcription regulator	25231
Prlr	Prolactin receptor	Plasma membrane	Transmembrane receptor	24684
Rims1	–	Unknown	Other	
Rrad	Ras-related associated with diabetes	Cytoplasm	Enzyme	83521
Set	SET nuclear oncogene	Nucleus	Phosphatase	307947
Slc1a6	Solute carrier family 1 (high affinity aspartate/glutamate transporter), member 6	Plasma membrane	Transporter	84012
Slc27a1	Solute carrier family 27 (fatty acid transporter), member 1	Plasma membrane	Transporter	94172
Slc4a1	Solute carrier family 4, anion exchanger, member 1	Plasma membrane	Transporter	24779
Slc8a2	Solute carrier family 8 (sodium/calcium exchanger), member 2	Cytoplasm	Transporter	140447
Srr	Serine racemase	Cytoplasm	Enzyme	303306
Stxbp1	Syntaxin binding protein 1	Cytoplasm	Transporter	25558

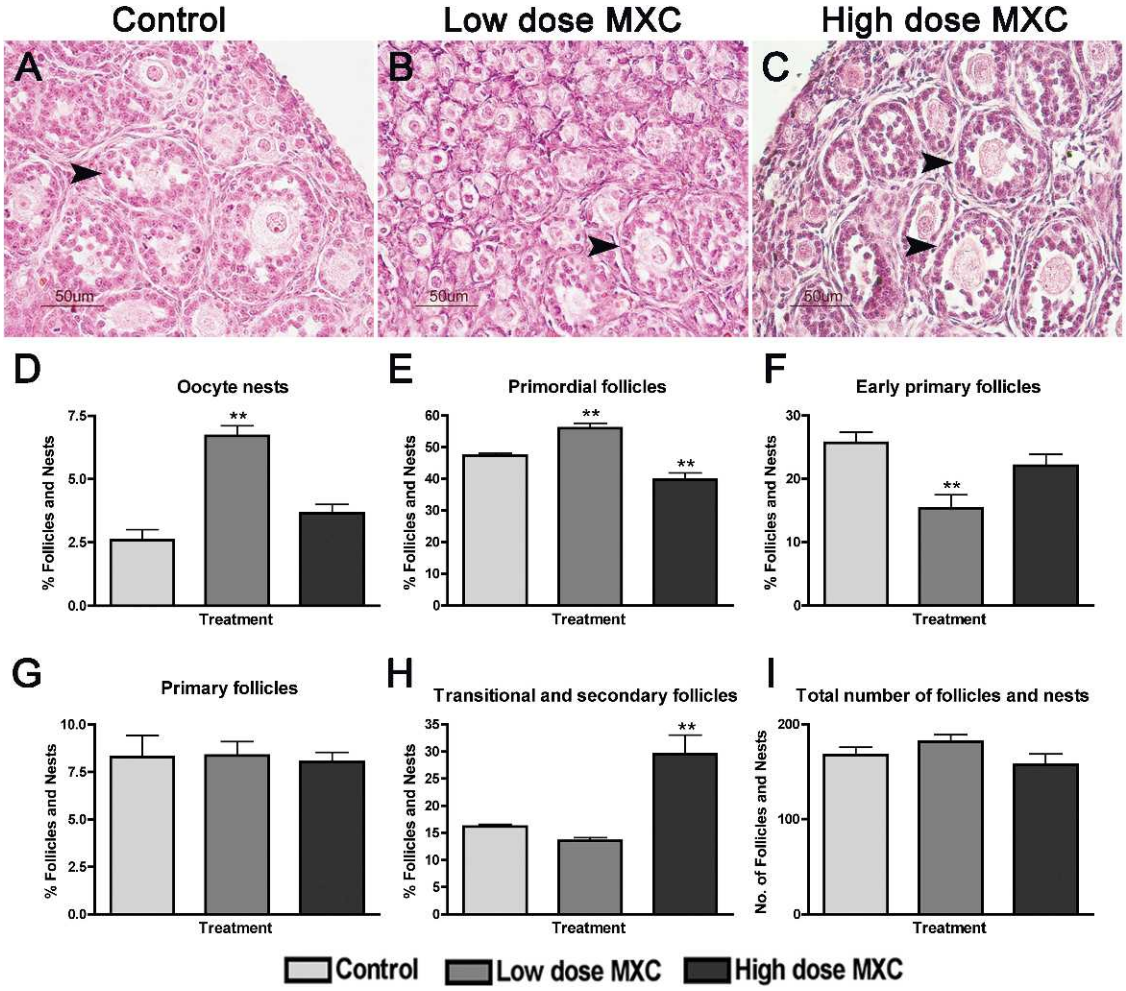

FIG. 1. Effect of fetal and neonatal MXC exposure on in vivo follicle stage composition in postnatal day (PND) 7 ovaries. Representative images of hematoxylin and eosin-stained histology of 5 μm ovary sections from PND 7 rats exposed during fetal and neonatal periods to vehicle (DMSO:oil [1:2], Control; **A**), 20 μg/kg/day MXC (low-dose MXC; **B**), and 100 mg/kg/day MXC (high-dose MXC; **C**). Primordial through secondary follicles (arrowhead) were observed in control, low-dose MXC, and high-dose MXC, but with a predominant number of primordial follicles and oocyte nests (**B**) in the low-dose MXC and increased numbers of transitional and secondary follicles in the high-dose MXC group. Bar = 50 μm. Follicles and nests were counted from the two largest serial sections selected from the center of the ovary and classified into oocyte nests (**D**), primordial follicles (**E**), early primary follicles (**F**), primary follicles (**G**), and transitional/secondary follicles (**H**). The area of each cross-section was measured with an optical micrometer, and the total follicles counted were normalized to the area of each cross-section (**I**). The percentage of oocyte nests or each follicle type was calculated based on the total number of follicles and nests per entire ovarian section. In addition, the entire nest, rather than each oocyte within the nest, was counted as one; n = 5–7 ovaries (animals) from at least three litters per treatment group. Error bars represent SEM. $^{**}P < 0.01$.

follicles and some primary follicles showed AMH expression in control ovaries (Fig. 2A). The staining intensities increased in the same stage of follicles in ovaries treated with low- and high-dose MXC (Fig. 2, B and C). We quantified the staining intensity of the entire ovary section of multiple animals from each treatment group, which showed that there was a significant increase of AMH expression in MXC-treated ovaries ($^{*}P < 0.05$, $^{**}P < 0.01$, Fig. 2D).

Examination of Genome-Wide Methylation Using Targeted Design Microarrays

To identify differences in genome-wide methylation patterns at PND 7 and 60 after low- and high-dose MXC treatment, we performed targeted array hybridizations with Nimblegen 3X720K CpG Island Plus RefSeq Promoter Arrays. We identified over 3000 methylation peaks in each of the samples, with methylation peak scores ranging from 2 to 8 (see *Materials and Methods* for details).

Functional Annotation of Methylation Events

The candidate loci were functionally annotated using IPA. Core analysis was conducted on each sample from each treatment group. The core analysis allows for the rapid assessment of the canonical signaling pathways, molecular networks, and biological processes that are most significantly perturbed in a given data set. All the loci with >2.00 assigned peak score in Nimblescan were annotated. Annotations were based on the Ingenuity Knowledge Base, and all the relationships (direct and indirect) were accounted for. Only data specific to the ovary or ovarian cell lines are presented.

There were 83 and 104 methylation events common to all the treatments at PND 7 and 60, respectively (Fig. 3, A and B). However, unique loci were also identified that were specific to low- and high-dose MXC treatments: 35 and 25 loci in low and high dose at PND 7 (Fig. 3A), and 42 and 36 loci in low and high dose at PND 60 (Fig. 3B).

The candidate loci were then examined for specific pathways with which they could be associated. Comparative

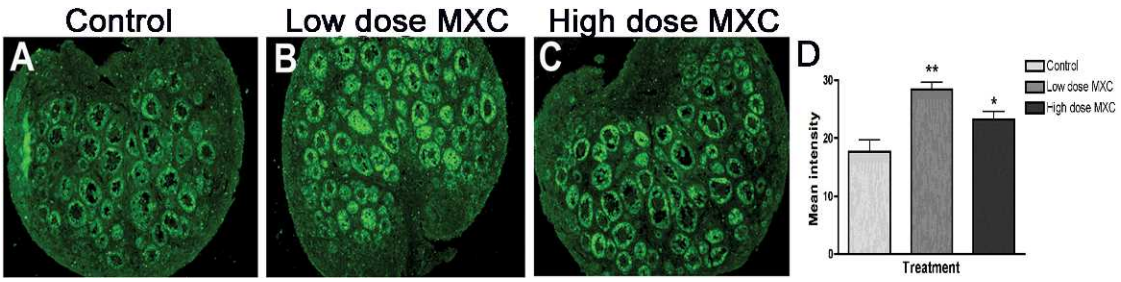

FIG. 2. The effect of fetal and neonatal MXC exposure on AMH expression in PND 7 ovaries. Representative images from immunohistochemical analysis of AMH in PND 7 rat ovaries treated with vehicle, (DMSO:oil [1:2], Control; **A**), 20 μg/kg/day MXC (low-dose MXC; **B**), and 100 mg/kg/day MXC (high-dose MXC; **C**). Original magnification ×100. Quantification of AMH expression was performed on the whole ovary area using Image J software (NIH Image). There was a significant increase in the levels of AMH in low-dose MXC-treated and high-dose MXC-treated ovaries (**D**). Analysis was conducted with four separate animals per treatment in each experiment from at least three different litters. Error bars represent SEM. $*P < 0.05$ and $**P < 0.01$.

canonical pathway details are presented in Figure 4, and the detailed candidate lists are in Tables 1 and 2. We found that at PND 60, the IGF-1 signaling, insulin receptor signaling, leptin signaling, and ERK/MAPK signaling pathways were among the pathways that had the highest *P*-value score with exclusive treatment effects with high-dose MXC. Numerous other pathways were similarly affected at PND 7, the most prominent ones being the estrogen-dependent breast cancer signaling, glucocorticoid receptor signaling, phosphatase and tensin homolog (PTEN) signaling, RhoA signaling, and PI3K/Akt signaling pathways. The ERK/MAPK pathway was affected at both PND 7 and 60. Pathways that were common to all the treatments are depicted in Supplemental Figure S1.

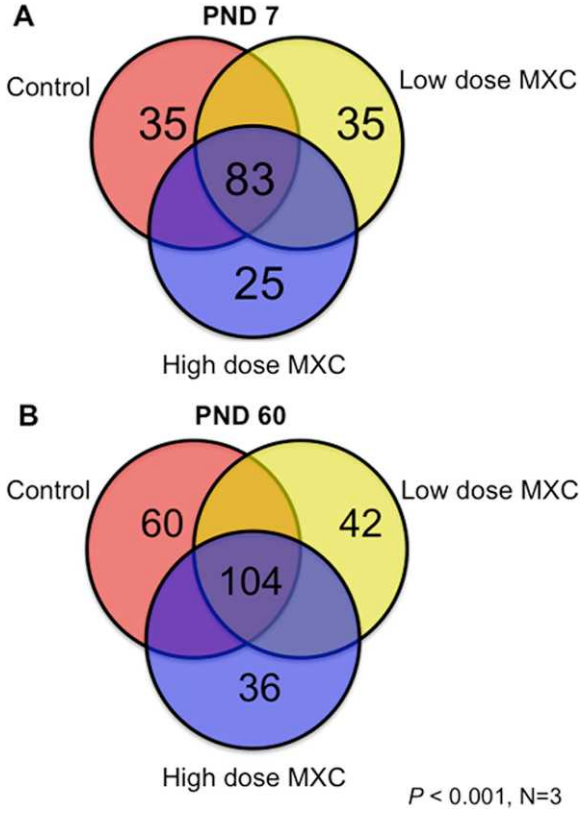

FIG. 3. The Venn diagram depicts unique and common methylation events to specific treatment groups as identified in Ingenuity Pathway Analysis: PND 7 (**A**) and PND 60 (**B**). Tables 1 and 2 contain the unique candidate loci details.

Gene Expression Analysis

To explore whether such hypermethylation events resulted in gene expression changes, we conducted a 96-gene TLDA analysis (Supplemental Table S1). Out of the 93 genes (excluding the controls), 23 genes were significantly downregulated ($P < 0.05$). Graphical representations are presented in Figure 5, while the tabular format is shown in Supplemental Table S2. Twelve genes, *Arnt, Atp5b, Cebpa, Dnmt3a, Foxo3a, Fst, Gnas, Insr, Prkca, Slc27a1, Smad2,* and *Lpar1* (not shown), were downregulated in PND 60 high-dose MXC samples only while five other genes, *Pgr, Igfbp5, Prkcb, Runx2, Cdkn1a,* and *Cav1* were downregulated at PND 7. Interestingly, *Cyp26b1* was the only gene whose expression was upregulated at PND 7. There were genes common to both ages that were downregulated such as *Cyp1b1, Hras, Hsd17b7, Igf1r, Max,* and *PI3kr1*. These results suggested that there was not a one to one correlation between hypermethylation and gene expression, that is, some loci were hypermethylated yet the gene expression was not affected (~75% of the total number of hypermethylated loci that were assayed for gene expression). On the other hand, several of the genes that were downregulated are highly pertinent to estrogen metabolism (e.g., *Cyp1b1, Hsd17b7*), folliculogenesis (e.g., *Foxo3, Fst, Pi3kr*), ovulation (e.g., *Cebpa, Pi3kr, Igf1r, Pgr*), and luteinization (e.g., *Runx2*).

DISCUSSION

Our previous studies examined the detrimental effects of fetal and neonatal MXC exposure on PND 60 ovaries. In this article, we demonstrate via a targeted genome-wide methylation analysis that there are multiple loci in the ovarian epigenome belonging to critically important signaling pathways that are hypermethylated by such exposure. Immediate changes in early folliculogenesis were also observed at PND 7 that correlated with the hypermethylation events. Furthermore, while a majority of the molecules and pathways were very specific to the treatment group and the age of the animals, some key players that were hypermethylated (at either age) had lower gene expression at both PND 7 and 60. Together, these data suggest that developmental EDC exposure can have an age-dependent impact on the ovarian epigenome and gene expression that are likely to cause specific defects in ovarian development and function.

Immediate Effects on Neonatal Ovaries and Delayed Effects on Adult Ovaries

Neonatal ovaries from high-dose MXC-treated animals had a markedly different phenotype than low-dose MXC-treated ovaries. In the latter, oocyte nest and primordial follicle numbers were increased with a concomitant decrease in early

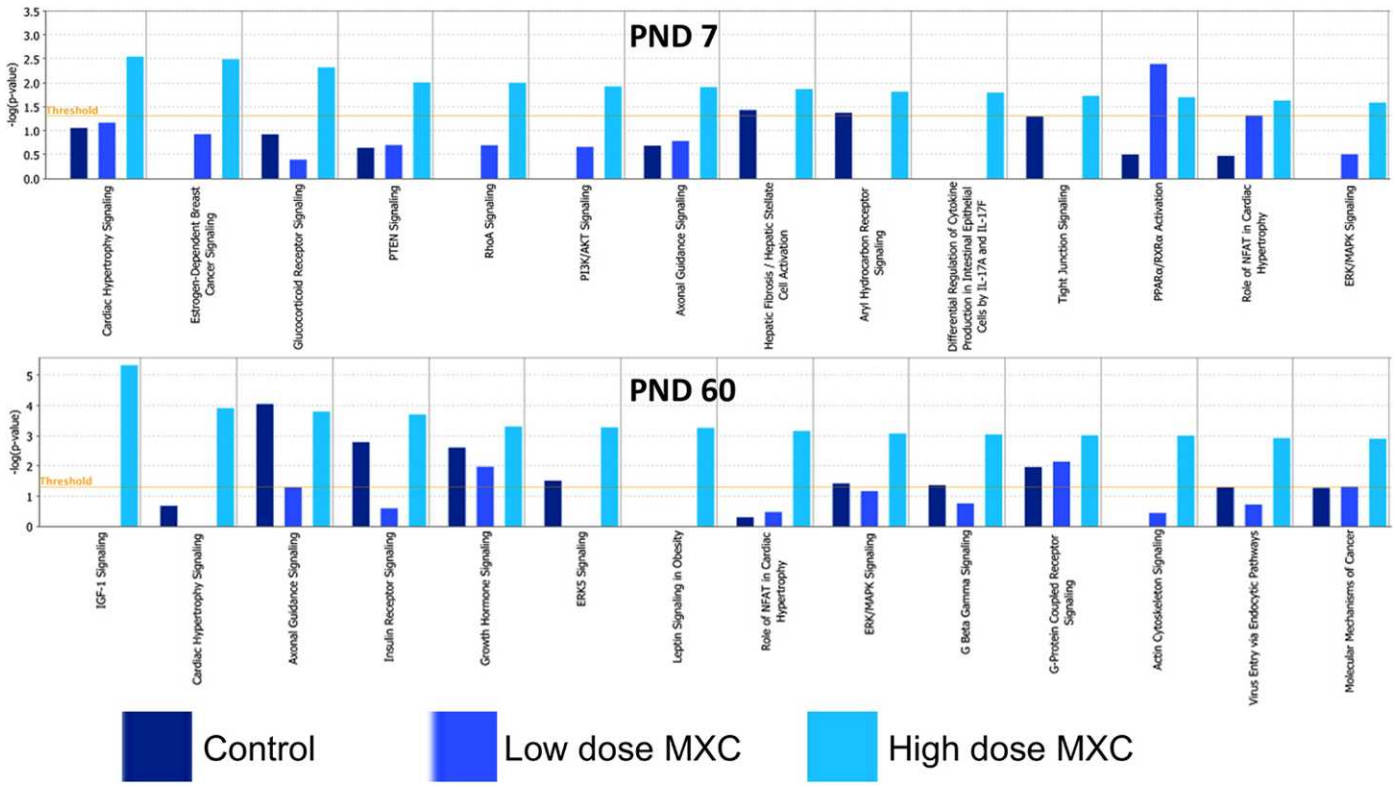

FIG. 4. Ingenuity Pathway Analysis was utilized to identify canonical pathways that were significantly associated with the hypermethylated candidate loci in PND 7 and 60 day old ovaries from animals treated with vehicle (control), 20 μg/kg/day (low-dose MXC), and 100 mg/kg/day (high-dose MXC), between E19 and PND 7, as described in *Materials and Methods*. Briefly, the significance of the association between the candidate data set and a given canonical pathway was measured by calculating the ratio between the number of molecules from our data sets that map to that particular pathway and the number of all molecules that map to the same pathway. Fisher exact test was used to calculate a P value indicating the probability that the association between the genes in the data set and the canonical pathway is explained by chance alone. A $P < 0.05$ was considered significant.

primary follicles with no change in the numbers of transitional/secondary follicles, suggesting that low-dose MXC inhibited follicular assembly and/or initial recruitment. These data are consistent with studies with estradiol and genistein on neonatal mouse or rat ovaries showing that estradiol or estrogenic EDCs can cause an increase in MOFs by reducing oocyte nest breakdown/follicular assembly or an increase in primordial follicles but a reduction in primary follicles by reducing initial recruitment [9, 10, 12, 14, 33]. On the other hand, high-dose MXC exposure resulted in an increase in the percentage of transitional/secondary follicles while it reduced the percentage of primordial follicles, suggesting that it stimulates the initial recruitment and/or subsequent follicular growth. Recent studies with different doses of BPA have shown that the primordial follicle pool is diminished by a high dose of BPA with an increase in the later stages of follicles, suggesting that the initial recruitment is accelerated while the primordial pool is expanded at a low dose of BPA [30]. These results mirror the data from the current study, which suggest that the effects of EDCs on the female reproductive lifespan may be dependent on such early estrogenic/anti-estrogenic exposures. The fact that vastly different gene expression profiles are created with different doses of estrogen/estrogenic compounds has been well documented in other tissues as well [34–36].

The difference between the doses may be due to the possibility that MXC and/or its metabolites are estrogenic at the low dose and antiestrogenic at the high dose. MXC metabolizes into bis- and mono-OH-MXC, which are considered to be more potent than MXC. The levels/ratio of these metabolites could define the overall activity of MXC as being estrogenic versus antiestrogenic [37]. Future studies will determine the levels of each biologically active metabolite being produced from MXC in the neonates as previously reported in adult rats [38].

It was interesting that AMH levels were elevated in both low- and high-dose MXC-treated PND 7 ovaries, suggesting that AMH is a good marker for any perturbation of follicular composition and that the low-dose MXC-treated ovaries may begin expressing AMH at an earlier stage to suppress initial recruitment of primordial follicles into the primary stage while in high-dose ovaries the transitional/secondary follicles (whose numbers were elevated by the exposure) are the ones that are expressing AMH. In addition, *Amh* gene has estrogen-responsive elements in its promoter [39], suggesting that estrogenic or antiestrogenic compounds, including EDCs can affect AMH expression and, in turn, the process of initial recruitment [28, 40, 41]. Our previous study showed that low-dose MXC had limited or no effect on follicular composition in the adult ovaries, which suggests that the follicles recover from the early effects of low-dose MXC [4]. In contrast, the high-dose MXC exposure resulted in a significant increase in the numbers of preantral and early antral follicles, and a reduced number of ovulations, suggesting that the initial modifications in the follicular events may have had more long-lasting detrimental effects on adult folliculogenesis. DNA methylation analysis at the AMH promoter region in MXC-treated ovaries revealed hypermethylation at a single CpG site that is within the putative binding site of an estrogen-responsive, Kruppel-like transcription factor (Zama and Uzumcu, unpublished results). Further examination of the nexus between AMH expression and its epigenetic modification after EDC exposure is definitely warranted.

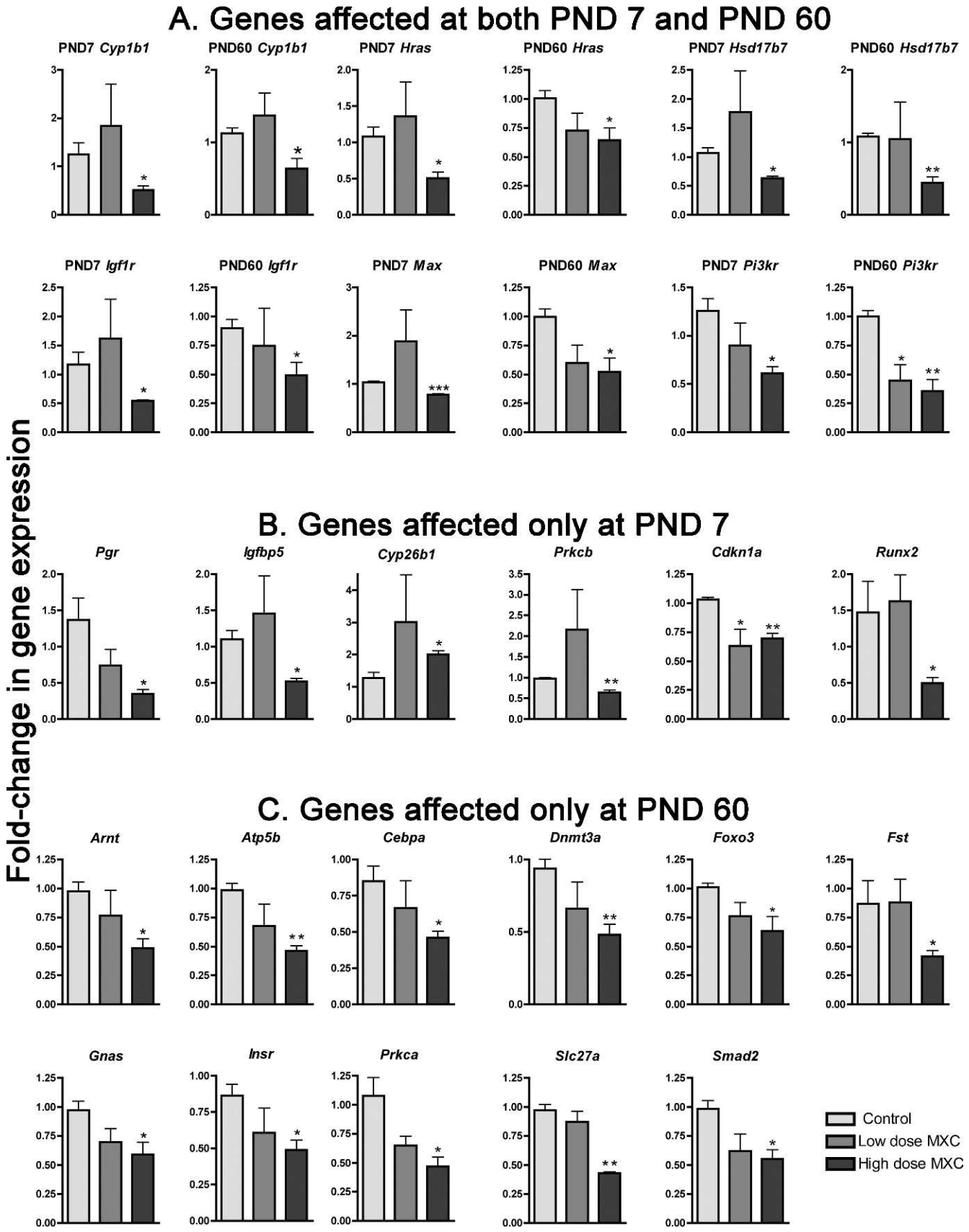

FIG. 5. Real-time quantitative PCR was conducted using TaqMan low-density array. Normalized gene expression of candidate genes that were affected at both PND 7 and PND 60 (**A**), PND 7 only (**B**), and PND 60 only (**C**) is presented. The control group was used as the calibrator group (Data Assist Software, Applied Bio Systems) and the false discovery rate calculated (Benjamini-Hochberg method, $P < 0.05$). A secondary *t*-test (two-tailed, nonparametric) was performed and *P* values reported. Error bars represent SEM. *$P < 0.05$, **$P < 0.01$, and ***$P < 0.001$.

TABLE 2. The genes that were hypermethylated in PND 60 ovaries by fetal and neonatal exposures to low dose (20 μg/kg) and high dose (100 mg/kg) of MXC.

Symbol	Entrez gene name	Location	Type(s)	Entrez gene ID for rat
High dose MXC				
Adrb2	Adrenergic, beta-2-, receptor, surface	Plasma membrane	G-protein coupled receptor	24176
Akap5	A kinase (PRKA) anchor protein 5	Plasma membrane	Other	171026
Ap2m1	Adaptor-related protein complex 2, mu 1 subunit	Cytoplasm	Transporter	116563
Cacna1a	Calcium channel, voltage-dependent, P/Q type, alpha 1A subunit	Plasma membrane	Ion channel	25398
Cd24	–	Unknown	Other	
Cdk16	Cyclin-dependent kinase 16	Cytoplasm	Kinase	81741
Ctf1	Cardiotrophin 1	Extracellular space	Cytokine	29201
Dbp	D site of albumin promoter (albumin D-box) binding protein	Nucleus	Transcription regulator	24309
Dio3	Deiodinase, iodothyronine, type III	Plasma membrane	Enzyme	29475
Dlg3	Discs, large homolog 3 (*Drosophila*)	Plasma membrane	Kinase	58948
Dusp1	Dual specificity phosphatase 1	Nucleus	Phosphatase	114856
Foxo3	Forkhead box O3	Nucleus	Transcription regulator	294515
Fst	Follistatin	Extracellular space	Other	24373
Gna12	Guanine nucleotide binding protein (G protein) alpha 12	Plasma membrane	Enzyme	81663
Hbegf	Heparin-binding EGF-like growth factor	Extracellular space	Growth factor	25433
Hprt1	Hypoxanthine phosphoribosyltransferase 1	Cytoplasm	Enzyme	24465
Hspb6	Heat shock protein, alpha-crystallin-related, B6	Cytoplasm	Other	192245
Ifngr2	Interferon gamma receptor 2 (interferon gamma transducer 1)	Plasma membrane	Transmembrane receptor	360697
Igf1r	Insulin-like growth factor 1 receptor	Plasma membrane	Transmembrane receptor	25718
Itsn1	Intersectin 1 (SH3 domain protein)	Cytoplasm	Other	29491
Lrrc8c	Leucine rich repeat containing 8 family, member C	Cytoplasm	Other	289443
Max	MYC associated factor X	Nucleus	Transcription regulator	60661
Pak3	p21 protein (Cdc42/Rac)-activated kinase 3	Cytoplasm	Kinase	29433
Pik3r1	Phosphoinositide-3-kinase, regulatory subunit 1 (alpha)	Cytoplasm	Other	25513
Ppard	Peroxisome proliferator-activated receptor delta	Nucleus	Ligand-dependent nuclear receptor	25682
Ppp1r9a	–	Unknown	Other	
Prkar2a	Protein kinase, cAMP-dependent, regulatory, type II, alpha	Cytoplasm	Kinase	29699
Psmd5	Proteasome (prosome, macropain) 26S subunit, non-ATPase, 5	Cytoplasm	Other	296651
Rab6a	RAB6A, member RAS oncogene family	Cytoplasm	Enzyme	84379
Runx2	Runt-related transcription factor 2	Nucleus	Transcription regulator	367218
Shank3	SH3 and multiple ankyrin repeat domains 3	Cytoplasm	Transcription regulator	59312
Socs3	Suppressor of cytokine signaling 3	Cytoplasm	Other	89829
Sstr2	Somatostatin receptor 2	Plasma membrane	G-protein coupled receptor	54305
Sstr3	Somatostatin receptor 3	Plasma membrane	G-protein coupled receptor	171044
Tubb6	Tubulin, beta 6	Cytoplasm	Other	307351
Wasf1	WAS protein family, member 1	Nucleus	Other	294568
Low dose MXC				
Accn3	Amiloride-sensitive cation channel 3	Plasma membrane	Ion channel	286920
Begain	Brain-enriched guanylate kinase-associated homolog (rat)	Nucleus	Other	79146
Caskin1	CASK interacting protein 1	Nucleus	Transcription regulator	140722
Ckap4	Cytoskeleton-associated protein 4	Cytoplasm	Other	362859
Crhr1	Corticotropin releasing hormone receptor 1	Plasma membrane	G-protein coupled receptor	58959
Cyp26b1	Cytochrome P450, family 26, subfamily B, polypeptide 1	Cytoplasm	Enzyme	312495
Dapk1	Death-associated protein kinase 1	Cytoplasm	Kinase	306722
Drd1	Dopamine receptor D1	Plasma membrane	G-protein coupled receptor	24316
Edn1	Endothelin 1	Extracellular space	Cytokine	24323
Gapdh	Glyceraldehyde-3-phosphate dehydrogenase	Cytoplasm	Enzyme	500983
Grin1	Glutamate receptor, ionotropic, N-methyl D-aspartate 1	Plasma membrane	Ion channel	24408
Hap1	Huntingtin-associated protein 1	Cytoplasm	Other	29430
Inppl1	Inositol polyphosphate phosphatase-like 1	Cytoplasm	Phosphatase	65038
Irf2	Interferon regulatory factor 2	Nucleus	Transcription regulator	290749
Kcnn2	Potassium intermediate/small conductance calcium-activated channel, subfamily N, member 2	Plasma membrane	Ion channel	54262
Ksr1	Kinase suppressor of ras 1	Cytoplasm	Kinase	360573
Lpar1	Lysophosphatidic acid receptor 1	Plasma membrane	G-protein coupled receptor	116744
Mafk	v-maf musculoaponeurotic fibrosarcoma oncogene homolog K (avian)	Nucleus	Transcription regulator	246760
Mag	Myelin associated glycoprotein	Plasma membrane	Other	29409
Magi2	Membrane associated guanylate kinase, WW and PDZ domain containing 2	Plasma membrane	Kinase	113970

TABLE 2. *Continued.*

Symbol	Entrez gene name	Location	Type(s)	Entrez gene ID for rat
Mapk8ip1	Mitogen-activated protein kinase 8 interacting protein 1	Cytoplasm	Other	116457
Ndn	Necdin homolog (mouse)	Nucleus	Other	308690
Nucb2	Nucleobindin 2	Nucleus	Other	59295
Ogt	*O*-linked N-acetylglucosamine (GlcNAc) transferase	Cytoplasm	Enzyme	26295
Orm1	–	Unknown	Other	
Pask	PAS domain containing serine/threonine kinase	Cytoplasm	Kinase	301617
Pde2a	Phosphodiesterase 2A, cGMP-stimulated	Cytoplasm	Enzyme	81743
Pdyn	Prodynorphin	Extracellular space	Transporter	29190
Pfn2	Profilin 2	Cytoplasm	Other	81531
Prkcb	Protein kinase C, beta	Cytoplasm	Kinase	25023
Ptpn6	Protein tyrosine phosphatase, non-receptor type 6	Cytoplasm	Phosphatase	116689
Qki	Quaking homolog, KH domain RNA binding (mouse)	Nucleus	Other	499022
Rbpjl	Recombination signal binding protein for immunoglobulin kappa J region-like	Nucleus	Transcription regulator	362268
Ren	Renin	Extracellular space	Peptidase	24715
Sdc3	Syndecan 3	Plasma membrane	Other	116673
Slc4a1	Solute carrier family 4, anion exchanger, member 1	Plasma membrane	Transporter	24779
Smad2	SMAD family member 2	Nucleus	Transcription regulator	29357
Stx1b	Syntaxin 1B	Plasma membrane	Ion channel	24923
Syngap1	Synaptic Ras GTPase activating protein 1	Plasma membrane	Other	192117
Syt2	Synaptotagmin II	Cytoplasm	Transporter	24805
Tgm2	Transglutaminase 2 (C polypeptide, protein-glutamine-gamma-glutamyltransferase)	Cytoplasm	Enzyme	56083
Th	Tyrosine hydroxylase	Cytoplasm	Enzyme	25085

Some Signaling Pathways Affected at PND 7 Mirror Those at PND 60 While Others Are Unique

As shown in Figure 6, the loci that were hypermethylated and exhibited a downregulation in gene expression were associated with canonical signaling pathways that intersected with multiple networks. For example, *Hras*, *Pik3r1*, *Igf1r*, *Insr*, *Foxo3a*, or *Prkca* are major signaling molecules in cardiac hypertrophy signaling, axonal guidance signaling, glucocorticoid signaling, and growth hormone signaling and yet occupy essential positions in ovarian-specific signaling pathways such as PTEN signaling, IGF-1 signaling, or rapid estrogen

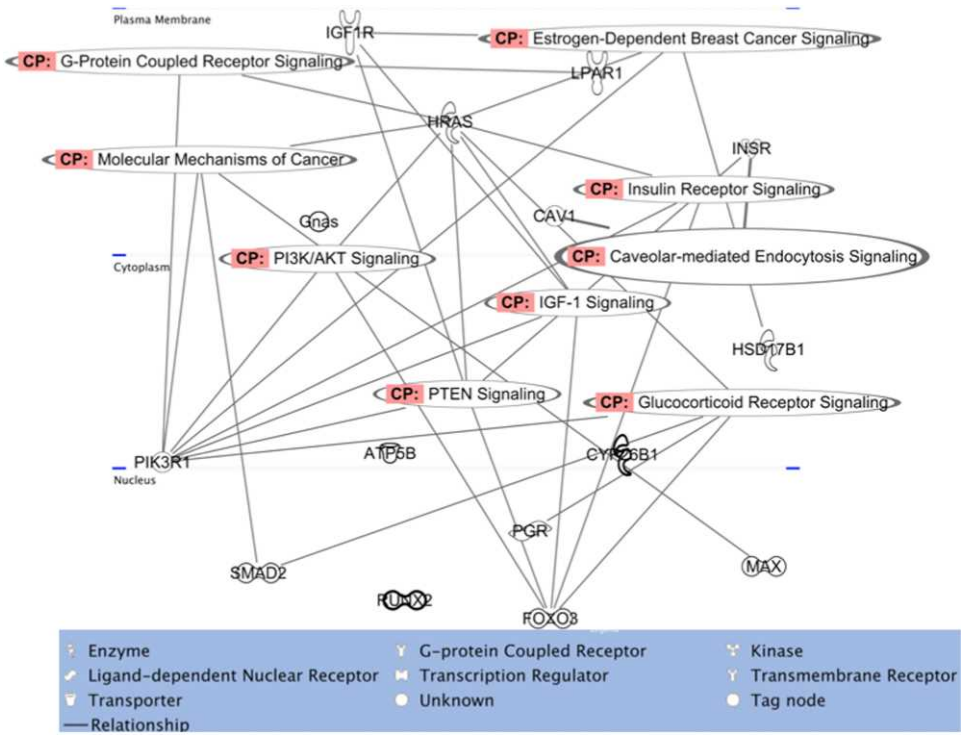

FIG. 6. The networks wherein various signaling pathways epigenetically affected by MXC exposure intersect and the relationships between affected molecules. Molecules are represented as nodes, and the biological relationship between two nodes is represented as an edge (line). All the edges are supported by at least one reference from the literature or from canonical information stored in the Ingenuity Pathways Knowledge Base. Human, mouse, and rat orthologs of a gene are stored as separate objects in the Ingenuity Pathways Knowledge Base but are represented as a single node in the network. Nodes are displayed using various shapes that represent the functional class of the gene product. CP = canonical signaling pathway.

signaling. Therefore, we examine the roles of these signaling molecules in the ovarian context.

Rapid estrogen signaling and PI3K signaling related molecules. It is now well-known that rapid estrogen signaling is implicated in cardiovascular function, neuroendocrine signaling, uterine signaling, and estrogen-dependent breast cancer signaling [42–45] and may very well be active in the ovary during folliculogenesis [33, 43]. This type of signaling involves a truncated version of ESR1, a membrane estrogen receptor (mER) protein, that has no intrinsic ability to signal because of the absence of structural domains with typical kinase activity and that is localized in pools near the plasma membrane. ESR1 is known to associate with other typical plasma membrane receptors such IGF1R and EGFR and promotes downstream signaling via a kinase cascade activation. One of the most prominent and well-studied of these pathways is the PI3K/Akt signaling pathway [46, 47]. Posttranslational modification of mER occurs upon ligand binding followed by localization to the cytoplasm and association with focal adhesion kinase, Src kinase, and the p85 subunit of PI3K [48]. We found that *Esr1* locus was hypermethylated at PND 7 in a region corresponding to its regulatory region. TLDA analysis suggested that there was no alteration in the levels of *Esr1,* and examination by immunofluorescence also found it to be unchanged. However, the antibody we utilized detected both nuclear and plasma membrane ESR1, and fine localization studies are yet to be conducted. Given that *Esr1* in neuroendocrine tissues is altered after estradiol exposure, it is imperative to fine dissect the methylation patterns of their regulatory regions in detail using pyrosequencing [6, 18]. Importantly, we found that at PND 60, the locus encoding *p85,* the regulatory subunit of PI3K (*Pi3kr1),* and *Igf1r* were both hypermethylated. Furthermore, the expression of both these genes was significantly reduced at both PND 7 and PND 60. These data suggest that the efficacy of the signaling pathway is inhibited soon after exposure and continues into adulthood. It is of significance that we found the hypermethylation in the locus encoding the regulatory subunit of PI3K (PI3KR1) and not the functional enzymatic subunit. PI3K signaling is common to numerous signaling responses and may affect ovarian functions as well [49, 50]. Studies of histone modifications after xenoestrogen exposures, in uteri, have supported our findings that EDC actions are mediated by epigenomic responses via PI3K signaling [51–53].

Aside from the PI3K signaling pathway, multiple candidates potentially involved in mER trafficking were identified at PND 7, albeit without significant gene expression changes. Caveolin 1 (CAV1) is a transporter of mER to the caveolar rafts in the plasma membrane [44] while HSP90AA1 is a chaperone protein that transports ESR1 to the nucleus for a typical DNA-dependent signaling event [54, 55]. *Hsp90aa1* was a candidate identified in the high-dose MXC-treated ovaries while *Cav1* was identified in the low-dose MXC-treated ovaries at PND 7. The differential association of ESR1 with CAV1 and HSP90AA1 may lead to entirely different signaling outcomes in the high and low doses. None of the above mentioned signaling/trafficking molecules were identified at PND 60, suggesting that these events were an early response to the treatment.

PTEN signaling. PTEN is a tumor suppressor protein that inhibits proliferation of granulosa cells and suppresses PI3K signaling [56]. The reversal of PTEN signaling also leads to premature primordial follicle activation in ovaries [57]. The oocyte-derived FOXO3 of the early stage follicles was shown to be a suppressor of the primordial to primary follicle transition [58]. When *Foxo3a* was deleted in mice, even though the initial primordial follicle pool was established normally, primordial follicles were activated in large numbers, leading to premature ovarian failure similar to the observations from the *Pten*-deleted mouse strain. Our data (Fig. 5 and Supplemental Table S2) show that *Foxo3, Pi3kr, Igf1r,* and *Hras,* belonging to the PTEN signaling pathway, as well as the PI3K/Akt signaling pathways were all hypermethylated and had lowered gene expression in the high-dose MXC-treated animals. This is associated with acceleration of folliculogenesis phenotype at PND 7 (current study) and a reduced ovulatory response and reproductive senescence in older animals [4]. While *Foxo3, Igf1r,* and *Pi3kr* were identified as hypermethylated in the PND 60 samples, the fact that they had reduced gene expression even at PND 7 makes it imperative that detailed epigenetic analysis be conducted on this signaling pathway.

IGF-1 signaling. There are many lines of evidence suggesting that follicle-stimulating hormone (FSH) stimulates IGF-1 signaling via PI3K/Akt signaling. One of the downstream effectors of this signaling pathway is FOXO3 (see above), expressed in the theca cells of preantral to later stage follicles as opposed to the oocyte-specific expression at earlier stages [59, 60]. FOXO3 is essential for theca cell and, later, luteal cell proliferation and differentiation. Therefore, hypermethylation and downregulation of its gene expression could cause the reduced ovulations as observed in high-dose MXC-treated animals at PND 60. Insulin-like growth factors (IGFs) are essential for follicular maturation because of their ability to stimulate granulosa cell proliferation and steroidogenesis, and *Igf1*-deficient mice show a very similar ovarian phenotype as FSH-KO mice [61–64]. In contrast, IGF-binding proteins (IGFBPs) can suppress FSH-induced follicular growth and differentiation, leading to atresia, possibly by sequestering IGF-1 protein and inhibiting its activity [65, 66]. FSH stimulates proteases that degrade IGFBPs, thereby increasing the bioavailability of IGFs. One such protease is pregnancy-associated plasma protein-A (PAPP-A), and high levels of its expression have been considered a marker of selected follicles [67]. We previously identified *Pappa* as a hypermethylated candidate locus (by AP-PCR) and showed that is epigenetically regulated by MXC exposure [5]. In the current study, we found *Pappa* to be hypermethylated in only two of the three replicates and therefore did not include it in the final candidate list. Together, these data suggest that hypermethylation of *Igf1r, Pi3kr,* and *Foxo3* have an effect on follicular maturation that is supported by the fact that there are reduced ovulations in MXC-treated ovaries.

One limitation with interpretation of the data from the whole ovary epigenome is that the ovary is heterogeneous and contains both gonadotropin-dependent and -independent follicles contributing to a varied epigenomic signature. Therefore, isolation of follicles of each stage and examination of the follicle stage-specific, cell-specific, and treatment-specific DNA methylation and gene expression patterns of the candidates is necessary. Nonetheless, it is to be noted that the overwhelming representation is from the somatic cells (granulosa and theca cells), whose genome is known to be altered during early ovarian development [68]. Additionally, some DNA methylation events were inversely correlated with gene expression changes, while others were not, suggesting involvement of other epigenetic mechanisms. Recent work suggests that trimethylation of lysine 9 of histone 3, a repressive histone mark, increases in antral follicles of high- and low-dose MXC-treated follicles (Zama and Uzumcu, unpublished results). Overall, the current study combined with our previous studies [4, 5] shows that developmental MXC exposure induces direct and immediate ovarian dysfunction,

leading to female infertility. These effects are potentially mediated by dose- and age-dependent epigenetic alterations of genes that belong to critical signaling pathways in the ovary. The major strength of this study is that MXC is a model EDC [69], and other relevant EDCs may have similar epigenetic effects as shown in this study.

ACKNOWLEDGMENT

The authors wish to thank Dr. Kathy Manger for her assistance in the preparation of this manuscript, Dr. Andrea Gore for her critical reading of the manuscript, Drs. Qi Wang and Andrew Brooks of the Bionomics Research and Technology Center of Rutgers University for technical services, and Dr. Jason Marano for technical assistance.

REFERENCES

1. Barker DJ. The developmental origins of adult disease. Eur J Epidemiol 2003; 18:733–736.
2. Crain DA, Janssen SJ, Edwards TM, Heindel J, Ho SM, Hunt P, Iguchi T, Juul A, McLachlan JA, Schwartz J, Skakkebaek N, Soto AM, et al. Female reproductive disorders: the roles of endocrine-disrupting compounds and developmental timing. Fertil Steril 2008; 90:911–940.
3. Zama AM, Uzumcu M. Epigenetic effects of endocrine-disrupting chemicals on female reproduction: an ovarian perspective. Front Neuroendocrinol 2010; 31:420–439.
4. Armenti AE, Zama AM, Passantino L, Uzumcu M. Developmental methoxychlor exposure affects multiple reproductive parameters and ovarian folliculogenesis and gene expression in adult rats. Toxicol Appl Pharmacol 2008; 233:286–296.
5. Zama AM, Uzumcu M. Fetal and neonatal exposure to the endocrine disruptor methoxychlor causes epigenetic alterations in adult ovarian genes. Endocrinology 2009; 150:4681–4691.
6. Gore AC, Walker DM, Zama AM, Armenti AE, Uzumcu M. Early life exposure to endocrine-disrupting chemicals causes lifelong molecular reprogramming of the hypothalamus and premature reproductive aging. Mol Endocrinol 2011; 25:2157–2168.
7. Fuortes L, Clark MK, Kirchner HL, Smith EM. Association between female infertility and agricultural work history. Am J Ind Med 1997; 31: 445–451.
8. Younglai EV, Holloway AC, Foster WG. Environmental and occupational factors affecting fertility and IVF success. Hum Reprod Update 2005; 11: 43–57.
9. Chen Y, Jefferson WN, Newbold RR, Padilla-Banks E, Pepling ME. Estradiol, progesterone, and genistein inhibit oocyte nest breakdown and primordial follicle assembly in the neonatal mouse ovary in vitro and in vivo. Endocrinology 2007; 148:3580–3590.
10. Kezele P, Skinner MK. Regulation of ovarian primordial follicle assembly and development by estrogen and progesterone: endocrine model of follicle assembly. Endocrinology 2003; 144:3329–3337.
11. Skinner MK. Regulation of primordial follicle assembly and development. Hum Reprod Update 2005; 11:461–471.
12. Jefferson W, Newbold R, Padilla-Banks E, Pepling M. Neonatal genistein treatment alters ovarian differentiation in the mouse: inhibition of oocyte nest breakdown and increased oocyte survival. Biol Reprod 2006; 74: 161–168.
13. Iguchi T, Takasugi N. Polyovular follicles in the ovary of immature mice exposed prenatally to diethylstilbestrol. Anat Embryol (Berl) 1986; 175: 53–55.
14. Kirigaya A, Kim H, Hayashi S, Chambon P, Watanabe H, Lguchi T, Sato T. Involvement of estrogen receptor beta in the induction of polyovular follicles in mouse ovaries exposed neonatally to diethylstilbestrol. Zoolog Sci 2009; 26:704–712.
15. Gaido KW, Leonard LS, Maness SC, Hall JM, McDonnell DP, Saville B, Safe S. Differential interaction of the methoxychlor metabolite 2,2–bis-(p-hydroxyphenyl)-1,1,1-trichloroethane with estrogen receptors alpha and beta. Endocrinology 1999; 140:5746–5753.
16. Gaido KW, Maness SC, McDonnell DP, Dehal SS, Kupfer D, Safe S. Interaction of methoxychlor and related compounds with estrogen receptor alpha and beta, and androgen receptor: structure-activity studies. Mol Pharmacol 2000; 58:852–858.
17. Luense LJ, Veiga-Lopez A, Padmanabhan V, Christenson LK. Developmental programming: gestational testosterone treatment alters fetal ovarian gene expression. Endocrinology 2011; 152:4974–4983.
18. Schwarz JM, Nugent BM, McCarthy MM. Developmental and hormone-induced epigenetic changes to estrogen and progesterone receptor genes in brain are dynamic across the life span. Endocrinology 2010; 151: 4871–4881.
19. Reik W, Dean W, Walter J. Epigenetic reprogramming in mammalian development. Science 2001; 293:1089–1093.
20. Hajkova P, Erhardt S, Lane N, Haaf T, El-Maarri O, Reik W, Walter J, Surani MA. Epigenetic reprogramming in mouse primordial germ cells. Mech Dev 2002; 117:15–23.
21. Coffigny H, Bourgeois C, Ricoul M, Bernardino J, Vilain A, Niveleau A, Malfoy B, Dutrillaux B. Alterations of DNA methylation patterns in germ cells and Sertoli cells from developing mouse testis. Cytogenet Cell Genet 1999; 87:175–181.
22. Ueda T, Abe K, Miura A, Yuzuriha M, Zubair M, Noguchi M, Niwa K, Kawase Y, Kono T, Matsuda Y, Fujimoto H, Shibata H, et al. The paternal methylation imprint of the mouse H19 locus is acquired in the gonocyte stage during foetal testis development. Genes Cells 2000; 5:649–659.
23. Obata Y, Kono T. Maternal primary imprinting is established at a specific time for each gene throughout oocyte growth. J Biol Chem 2002; 277: 5285–5289.
24. Stouder C, Paoloni-Giacobino A. Specific transgenerational imprinting effects of the endocrine disruptor methoxychlor on male gametes. Reproduction 2011; 141:207–216.
25. Kouzmenko A, Ohtake F, Fujiki R, Kato S. Hormonal gene regulation through DNA methylation and demethylation. Epigenomics 2010; 2: 765–774.
26. Gray LE Jr, Ostby J, Ferrell J, Rehnberg G, Linder R, Cooper R, Goldman J, Slott V, Laskey J. A dose-response analysis of methoxychlor-induced alterations of reproductive development and function in the rat. Fundam Appl Toxicol 1989; 12:92–108.
27. Chapin RE, Harris MW, Davis BJ, Ward SM, Wilson RE, Mauney MA, Lockhart AC, Smialowicz RJ, Moser VC, Burka LT, Collins BJ. The effects of perinatal/juvenile methoxychlor exposure on adult rat nervous, immune, and reproductive system function. Fundam Appl Toxicol 1997; 40:138–157.
28. Uzumcu M, Kuhn PE, Marano JE, Armenti AE, Passantino L. Early postnatal methoxychlor exposure inhibits folliculogenesis and stimulates anti-Mullerian hormone production in the rat ovary. J Endocrinol 2006; 191:549–558.
29. Nilsson E, Parrott JA, Skinner MK. Basic fibroblast growth factor induces primordial follicle development and initiates folliculogenesis. Mol Cell Endocrinol 2001; 175:123–130.
30. Rodriguez HA, Santambrosio N, Santamaria CG, Munoz-de-Toro M, Luque EH. Neonatal exposure to bisphenol A reduces the pool of primordial follicles in the rat ovary. Reprod Toxicol 2010; 30:550–557.
31. Ruegg J, Swedenborg E, Wahlstrom D, Escande A, Balaguer P, Pettersson K, Pongratz I. The transcription factor aryl hydrocarbon receptor nuclear translocator functions as an estrogen receptor beta-selective coactivator, and its recruitment to alternative pathways mediates antiestrogenic effects of dioxin. Mol Endocrinol 2008; 22:304–316.
32. Swedenborg E, Pongratz I. AhR and ARNT modulate ER signaling. Toxicology 2010; 268:132–138.
33. Chen Y, Breen K, Pepling ME. Estrogen can signal through multiple pathways to regulate oocyte cyst breakdown and primordial follicle assembly in the neonatal mouse ovary. J Endocrinol 2009; 202:407–417.
34. Coser KR, Chesnes J, Hur J, Ray S, Isselbacher KJ, Shioda T. Global analysis of ligand sensitivity of estrogen inducible and suppressible genes in MCF7/BUS breast cancer cells by DNA microarray. Proc Natl Acad Sci U S A 2003; 100:13994–13999.
35. Hewitt SC, O'Brien JE, Jameson JL, Kissling GE, Korach KS. Selective disruption of ER{alpha} DNA-binding activity alters uterine responsiveness to estradiol. Mol Endocrinol 2009; 23:2111–2116.
36. Deroo BJ, Hewitt SC, Collins JB, Grissom SF, Hamilton KJ, Korach KS. Profile of estrogen-responsive genes in an estrogen-specific mammary gland outgrowth model. Mol Reprod Dev 2009; 76:733–750.
37. Alworth LC, Howdeshell KL, Ruhlen RL, Day JK, Lubahn DB, Huang TH, Besch-Williford CL, vom Saal FS. Uterine responsiveness to estradiol and DNA methylation are altered by fetal exposure to diethylstilbestrol and methoxychlor in CD-1 mice: effects of low versus high doses. Toxicol Appl Pharmacol 2002; 183:10–22.
38. Ohyama K, Maki S, Sato K, Kato Y. Comparative in vitro metabolism of the suspected pro-oestrogenic compound, methoxychlor in precision-cut liver slices from male and female rats. Xenobiotica 2005; 35:331–342.
39. Guerrier D, Boussin L, Mader S, Josso N, Kahn A, Picard JY. Expression of the gene for anti-Mullerian hormone. J Reprod Fertil 1990; 88:695–706.
40. Ikeda Y, Nagai A, Ikeda MA, Hayashi S. Neonatal estrogen exposure inhibits steroidogenesis in the developing rat ovary. Dev Dyn 2001; 221: 443–453.
41. Ikeda Y, Nagai A, Ikeda MA, Hayashi S. Increased expression of

Mullerian-inhibiting substance correlates with inhibition of follicular growth in the developing ovary of rats treated with E2 benzoate. Endocrinology 2002; 143:304–312.
42. McDevitt MA, Glidewell-Kenney C, Jimenez MA, Ahearn PC, Weiss J, Jameson JL, Levine JE. New insights into the classical and non-classical actions of estrogen: evidence from estrogen receptor knock-out and knock-in mice. Mol Cell Endocrinol 2008; 290:24–30.
43. Pedram A, Razandi M, Kim JK, O'Mahony F, Lee EY, Luderer U, Levin ER. Developmental phenotype of a membrane only estrogen receptor alpha (MOER) mouse. J Biol Chem 2009; 284:3488–3495.
44. Pedram A, Razandi M, Sainson RC, Kim JK, Hughes CC, Levin ER. A conserved mechanism for steroid receptor translocation to the plasma membrane. J Biol Chem 2007; 282:22278–22288.
45. Razandi M, Pedram A, Merchenthaler I, Greene GL, Levin ER. Plasma membrane estrogen receptors exist and functions as dimers. Mol Endocrinol 2004; 18:2854–2865.
46. Simoncini T, Rabkin E, Liao JK. Molecular basis of cell membrane estrogen receptor interaction with phosphatidylinositol 3-kinase in endothelial cells. Arterioscler Thromb Vasc Biol 2003; 23:198–203.
47. Tian J, Berton TR, Shirley SH, Lambertz I, Gimenez-Conti IB, DiGiovanni J, Korach KS, Conti CJ, Fuchs-Young R. Developmental stage determines estrogen receptor alpha expression and non-genomic mechanisms that control IGF-1 signaling and mammary proliferation in mice. J Clin Invest 2012; 122:192–204.
48. Levin ER. Minireview: extranuclear steroid receptors: roles in modulation of cell functions. Mol Endocrinol 2011; 25:377–384.
49. Santen RJ, Fan P, Zhang Z, Bao Y, Song RX, Yue W. Estrogen signals via an extra-nuclear pathway involving IGF-1R and EGFR in tamoxifen-sensitive and -resistant breast cancer cells. Steroids 2009; 74:586–594.
50. Song RX, Chen Y, Zhang Z, Bao Y, Yue W, Wang JP, Fan P, Santen RJ. Estrogen utilization of IGF-1-R and EGF-R to signal in breast cancer cells. J Steroid Biochem Mol Biol 2010; 118:219–230.
51. Doherty LF, Bromer JG, Zhou Y, Aldad TS, Taylor HS. In utero exposure to diethylstilbestrol (DES) or bisphenol-A (BPA) increases EZH2 expression in the mammary gland: an epigenetic mechanism linking endocrine disruptors to breast cancer. Horm Cancer 2010; 1:146–155.
52. Bredfeldt TG, Greathouse KL, Safe SH, Hung MC, Bedford MT, Walker CL. Xenoestrogen-induced regulation of EZH2 and histone methylation via estrogen receptor signaling to PI3K/AKT. Mol Endocrinol 2010; 24: 993–1006.
53. Greathouse KL, Bredfeldt T, Everitt JI, Lin K, Berry T, Kannan K, Mittelstadt ML, Ho SM, Walker CL. Environmental estrogens differentially engage the histone methyltransferase EZH2 to increase risk of uterine tumorigenesis. Mol Cancer Res 2012; 10:546–557.
54. Sanchez ER. Chaperoning steroidal physiology: lessons from mouse genetic models of Hsp90 and its cochaperones. Biochim Biophys Acta 2012; 1823:722–729.
55. Powell E, Wang Y, Shapiro DJ, Xu W. Differential requirements of Hsp90 and DNA for the formation of estrogen receptor homodimers and heterodimers. J Biol Chem 2010; 285:16125–16134.
56. Fan HY, Liu Z, Cahill N, Richards JS. Targeted disruption of Pten in ovarian granulosa cells enhances ovulation and extends the life span of luteal cells. Mol Endocrinol 2008; 22:2128–2140.
57. Jagarlamudi K, Liu L, Adhikari D, Reddy P, Idahl A, Ottander U, Lundin E, Liu K. Oocyte-specific deletion of Pten in mice reveals a stage-specific function of PTEN/PI3K signaling in oocytes in controlling follicular activation. PLoS One 2009; 4:e6186.
58. Castrillon DH, Miao L, Kollipara R, Horner JW, DePinho RA. Suppression of ovarian follicle activation in mice by the transcription factor Foxo3a. Science 2003; 301:215–218.
59. Liu Z, Rudd MD, Hernandez-Gonzalez I, Gonzalez-Robayna I, Fan HY, Zeleznik AJ, Richards JS. FSH and FOXO1 regulate genes in the sterol/steroid and lipid biosynthetic pathways in granulosa cells. Mol Endocrinol 2009; 23:649–661.
60. Richards JS, Sharma SC, Falender AE, Lo YH. Expression of FKHR, FKHRL1, and AFX genes in the rodent ovary: evidence for regulation by IGF-I, estrogen, and the gonadotropins. Mol Endocrinol 2002; 16: 580–599.
61. Kwintkiewicz J, Giudice LC. The interplay of insulin-like growth factors, gonadotropins, and endocrine disruptors in ovarian follicular development and function. Semin Reprod Med 2009; 27:43–51.
62. Edson MA, Nagaraja AK, Matzuk MM. The mammalian ovary from genesis to revelation. Endocr Rev 2009; 30:624–712.
63. Mazerbourg S, Bondy CA, Zhou J, Monget P. The insulin-like growth factor system: a key determinant role in the growth and selection of ovarian follicles? a comparative species study. Reprod Domest Anim 2003; 38:247–258.
64. deMoura MD, Choi D, Adashi EY, Payne DW. Insulin-like growth factor-I-mediated amplification of follicle-stimulating hormone-supported progesterone accumulation by cultured rat granulosa cells: enhancement of steroidogenic enzyme activity and expression. Biol Reprod 1997; 56: 946–953.
65. Ui M, Shimonaka M, Shimasaki S, Ling N. An insulin-like growth factor-binding protein in ovarian follicular fluid blocks follicle-stimulating hormone-stimulated steroid production by ovarian granulosa cells. Endocrinology 1989; 125:912–916.
66. Cataldo NA, Woodruff TK, Giudice LC. Regulation of insulin-like growth factor binding protein production by human luteinizing granulosa cells cultured in defined medium. J Clin Endocrinol Metab 1993; 76:207–215.
67. Conover CA, Faessen GF, Ilg KE, Chandrasekher YA, Christiansen M, Overgaard MT, Oxvig C, Giudice LC. Pregnancy-associated plasma protein-a is the insulin-like growth factor binding protein-4 protease secreted by human ovarian granulosa cells and is a marker of dominant follicle selection and the corpus luteum. Endocrinology 2001; 142:2155.
68. Hoivik EA, Aumo L, Aesoy R, Lillefosse H, Lewis AE, Perrett RM, Stallings NR, Hanley NA, Bakke M. Deoxyribonucleic acid methylation controls cell type-specific expression of steroidogenic factor 1. Endocrinology 2008; 149:5599–5609.
69. Cummings AM. Methoxychlor as a model for environmental estrogens. Crit Rev Toxicol 1997; 27:367–379.

ED: Please verify the accuracy of any edits made to the article summary below.

Developmental exposure to the model endocrine-disrupting chemical methoxychlor leads to age-dependent alterations in DNA methylation patterns in multiple signaling molecules, resulting in ovarian dysfunction in adulthood.